NANOSYSTEMS:
PHYSICS, CHEMISTRY, MATHEMATICS

Haneche N., et al. *Nanosystems: Phys. Chem. Math.*, 2025, **16** (4), 395–406.
http://nanojournal.ifmo.ru
DOI 10.17586/2220-8054-2025-16-4-395-406

Original article

A four-wing hyperchaotic attractor generated based on the Qi chaotic system and its application to high-speed encryption

Nabil Haneche[1,a], Tayeb Hamaizia[2,b]

[1]Applied Mathematics and Modeling Laboratory, Department of Mathematics, University of Mentouri Brothers, Constantine, 25000, Algeria

[2]Mathematical Modeling and Simulation Laboratory, Department of Mathematics, University of Mentouri Brothers, Constantine, 25000, Algeria

[a]nabil.haneche@doc.umc.edu.dz, [b]el.tayyeb@umc.edu.dz

Corresponding author: N. Haneche, nabil.haneche@doc.umc.edu.dz

PACS 05.45.-a, 05.45.Ac, 05.45.Vx, 89.70.Cf

ABSTRACT Recently, chaos theory and its applications have garnered the attention of many scholars. In this paper, a novel 4D dynamical system that can generate a four-wing hyperchaotic attractor and a double-wing chaotic attractor is presented. The dynamical behavior of this system is investigated using several numerical tools, including bifurcation diagrams, the spectrum of Lyapunov exponents, and phase plots. It is shown that the proposed system has multiple positive Lyapunov exponents for a wide range of parameters, which establishes its hyperchaotic behavior. Additionally, the multistability of this system is analyzed carefully through the coexistence of periodic, chaotic, and hyperchaotic attractors. The hyperchaotic patterns of this system render it suitable for encrypting multimedia data. An efficient, fast, and secure audio cryptographic algorithm is developed based on the hyperchaotic sequences generated from this system. Experimental tests are carried out to verify the performance and security of the proposed encryption method.

KEYWORDS Hyperchaotic system, Four-wing attractor, Multistability, Audio encryption.

ACKNOWLEDGEMENTS The authors would like to express their sincere thanks to the editor and the anonymous reviewers for their helpful comments and suggestions.

FOR CITATION Haneche N., Hamaizia T. A four-wing hyperchaotic attractor generated based on the Qi chaotic system and its application to high-speed encryption. *Nanosystems: Phys. Chem. Math.*, 2025, **16** (4), 395–406.

1. Introduction

Chaos theory, first discovered by physicist Henri Poincaré as early as in the 19-th century and later established by meteorologist Edward Lorenz, has gained significant attention over the past thirty years [1, 2]. It has been used to construct and generate dissipative and conservative chaotic systems, such as the antimonotonic hyperjerk system presented by Zambrano-Serrano et al. in 2021 [3], the imbalanced Hindmarsh-Rose neuron model by Zhang et al. [4], and a hyperchaotic coexistence attractor proposed by Yan et al. [5]. Bao et al. developed a no-argument memristive hyperjerk system with coexisting chaotic bubbles in 2022 [6]. These contributions have greatly enhanced chaos theory in systems design approaches and practical applications. However, some systems still exhibit restrictions in natural qualities and dynamic complexity. Chaotic systems have various applications due to their complex patterns. Chaotic systems are practically employed in several fields, including mathematical modeling [7], physics [8], chemistry [9], nanoscience [10–13], lasers [14], neural networks [15], signal processing [16], and secure communication [17].

Recent research highlights the differences between low- and high-dimensional chaotic systems. Low-dimensional systems, with no positive Lyapunov exponents, produce simple dynamics, potentially impairing information security. However, high-dimensional systems, with four dimensions or more, show two or more positive Lyapunov exponents, improving complexity, randomness, and resilience in secure applications [18]. Research has been influenced by the emergence of hyperchaotic autonomous systems with at least four-dimensional phase space, dissipative features, and multiple positive Lyapunov exponents. Hyperchaotic systems are beneficial in various fields, including random number generation, secure communication, synchronization, audio, video, and image encryption [19–22]. Hyperchaotic encryption offers benefits in stealth, dynamic flexibility, and computing efficiency, as well as processing speed for both stationary data storage and real-time applications. It generates powerful, security-oriented ciphertexts resistant to decoding attempts. Using chaos theory with audio encryption leads to new ideas for safe communication, making it fast and secure for transmitting sensitive audio [23].

In the context of nanoscience, hyperchaotic systems, with their complex dynamics characterized by multiple positive Lyapunov exponents and high complexity, offer promising applications in nanoscience for secure communication and data protection in nano-networks. Its hyperchaoticity can be harnessed to generate robust encryption keys for safeguarding sensitive information transmitted between nanodevices, such as in biomedical nanosensors or connected nanodevices. The system's inherent sensitivity to initial conditions and parameter variations ensures resilience against eavesdropping, making it ideal for low-power, high-security nanoscale environments where traditional cryptographic methods may be computationally prohibitive. This integration enhances both the confidentiality and integrity of data in next-generation nanotechnology applications.

The rest of this paper is organized as follows: In Section 2, the construction and dynamical analysis of the novel 4D hyperchaotic system are presented. In Section 3, the application of the proposed hyperchaotic system in secure audio encryption and decryption is performed. In Section 4, experimental tests and statistical metrics are carried out to demonstrate the performance and security of the developed chaos-based audio cryptosystem.

2. Generation and dynamical analysis of a new 4D hyperchaotic system

In 2008, Qi et al. introduced a new 3D four-wing chaotic system described as [24]:

$$\begin{cases} \dot{x} = -ax + ay + eyz, \\ \dot{y} = -xz + cx + dy, \\ \dot{z} = xy - bz, \end{cases} \tag{1}$$

where a, b, d, $e \in \mathbb{R}^+$ and $c \in \mathbb{R}$ are the system constant parameters. Inspired by the original Qi chaotic system, with the aim of obtaining richer dynamics and high complexity, we present a novel 4D hyperchaotic system that is constructed by adding a state feedback controller, w, as follows:

$$\begin{cases} \dot{x} = -ax + ew + yz, \\ \dot{y} = cy + xz, \\ \dot{z} = bz + fw - xy, \\ \dot{w} = dw - gz, \end{cases} \tag{2}$$

where a, b, d, e, f, $g \in \mathbb{R}^+$ and $c \in \mathbb{R}$ are the system constant parameters. The system (2) with ten terms has three quadratic nonlinearities and seven control parameters.

2.1. Symmetry

System (2) is symmetric with respect to the y-axis, i.e., it is invariant under the following coordinate transformations:

$$(x, y, z, w) \to (-x, y, -z, -w). \tag{3}$$

2.2. Dissipation

The vector field of the state space of system (2) is represented as

$$\mathbf{V} = \begin{bmatrix} \dot{x} \\ \dot{y} \\ \dot{z} \\ \dot{w} \end{bmatrix} = \begin{bmatrix} -ax + ew + yz \\ cy + xz \\ bz + fw - xy \\ dw - gz \end{bmatrix}. \tag{4}$$

Thus, the divergence of system (2) can be obtained as

$$\nabla \mathbf{V} = \frac{\partial \dot{x}}{\partial x} + \frac{\partial \dot{y}}{\partial y} + \frac{\partial \dot{z}}{\partial z} + \frac{\partial \dot{w}}{\partial w} = -a + b + c + d. \tag{5}$$

To ensure the chaoticness of system (2), the general condition of dissipativity should be verified, i.e., $\nabla \mathbf{V} < 0$ or $a > b + c + d$. As a result, the volume contraction is expressed as

$$\frac{d\mathbf{V}(t)}{dt} = -\mathbf{V}(t), \tag{6}$$

where $\mathbf{V}_0 = \mathbf{V}(0)$ is the initial volume element. By integrating both sides of equation (6), we can obtain

$$\mathbf{V}(t) = \mathbf{V}_0 e^{-t}. \tag{7}$$

The negative divergence ensures exponential convergence as $t \to \infty$, meaning that the trajectory rates shrink to zero, resulting in a loss of volume in phase space over time, which leads to the existence of a strange attractor.

2.3. Equilibria and stability

The equilibria of system (2) can be obtained by solving the following system of equations:

$$\begin{cases} -ax + ew + yz = 0, \\ cy + xz = 0, \\ bz + fw - xy = 0, \\ dw - gz = 0. \end{cases} \tag{8}$$

We obtain the trivial equilibrium $O = (0, 0, 0, 0)$ and $x = \pm\sqrt{-c\left(b + \dfrac{fg}{d}\right)}$, $z = \dfrac{c\left(eg \pm \sqrt{e^2g^2 + 4ad(bd + fg)}\right)}{2\sqrt{-cd(bd + fg)}}$, $y = -\dfrac{xz}{c}$, $w = \dfrac{g}{d}z$. These components exist only under the following specific parameter conditions

$$\begin{gathered} -c\left(b + \frac{fg}{d}\right) \geq 0 \quad \text{(to ensure real } x\text{)}, \\ e^2g^2 + 4ad(bd + fg) \geq 0 \quad \text{(to ensure real } z\text{)}. \end{gathered} \tag{9}$$

Let $a = 50$, $b = 10$, $c = -16$, $d = 0.2$, $e = 10$, $f = 16$, and $g = 0.5$, the four other non-trivial equilibria, respectively denoted as

$$E_1 = (x_1, y_1, z_1, w_1), \quad E_2 = (x_2, y_2, z_2, w_2), \quad E_3 = (x_3, y_3, z_3, w_3), \quad E_4 = (x_4, y_4, z_4, w_4), \tag{10}$$

can be calculated as

$$\begin{aligned} E_1 &= (28.28, -64.04, -36.23, -90.58), \\ E_2 &= (-28.28, -64.04, 36.23, 90.58), \\ E_3 &= (28.28, 39.06, 22.09, 55.23), \\ E_4 &= (-28.28, 39.06, -22.09, -55.23). \end{aligned} \tag{11}$$

In order to investigate the stability of all the equilibria, we consider the Jacobian matrices with different equilibria and calculate their eigenvalues. The linearization of system (2) around an equilibrium point $E = (x, y, z, w)$ provides the following Jacobian matrix

$$J_E = \begin{bmatrix} -a & z & y & e \\ z & c & x & 0 \\ -y & -x & b & f \\ 0 & 0 & -g & d \end{bmatrix}. \tag{12}$$

The results of the calculation are shown in Table 2. Due to eigenvalues with positive real parts, all equilibrium points are unstable, in which O is a saddle point and E_1, E_2, E_3, and E_4 are all saddle-foci nodes.

TABLE 1. Eigenvalues for all equilibria of system (2)

λ	O	E_1	E_2	E_3	E_4
λ_1	-50	-58.21	-58.21	-49.88	-49.88
λ_2	-16	$2.15 + 7.89i$	$2.15 + 7.89i$	$4.20 + 6.34i$	$4.20 + 6.34i$
λ_3	1.10	$2.15 - 7.89i$	$2.15 - 7.89i$	$4.20 - 6.34i$	$4.20 - 6.34i$
λ_4	9.10	-4.33	-4.33	-6.92	-6.92

2.4. Dynamical analysis of the novel 4D system

This study examines the basic dynamics of the novel 4D system (2) via the analysis of the Lyapunov exponents spectrum, bifurcation diagrams, Kaplan-Yorke fractal dimension, and Poincaré sections. The Lyapunov exponents $L_i\,(i = 1, 2, 3, 4)$ will be calculated using the Wolf algorithm [25], which involves solving the system with the ode45 ODE solver and using Gram-Schmidt orthonormalization. The numerical simulations are conducted with the MATLAB software. The fourth-order Runge-Kutta integration method was used to solve the differential equations. All simulations are performed

using the initial condition $(x_0, y_0, z_0, w_0) = (1, 1, 1, 1)$, except as mentioned differently. The results are described as follows.

Let the control parameter c vary in the range $[-22, -1]$ with a step size of $\Delta c = 0.01$. Figure 1(a) depicts the spectrum of Lyapunov exponents for the 4D system (2) with respect to the parameter c. Whereas, Fig. (1)(b) displays the bifurcation diagram of state z with respect to parameter c. One can see that when $z \in [-22, -18.27)$, the system (2) exhibits regular dynamics, in which periodic orbits appear. The Lyapunov exponents, where there is no positive Lyapunov exponent, validate this result. However, when $c \in [-18.27, -3.59]$, $L_1 > 0$, $L_2 > 0$, $L_3 = 0$, and $L_4 < 0$, which means

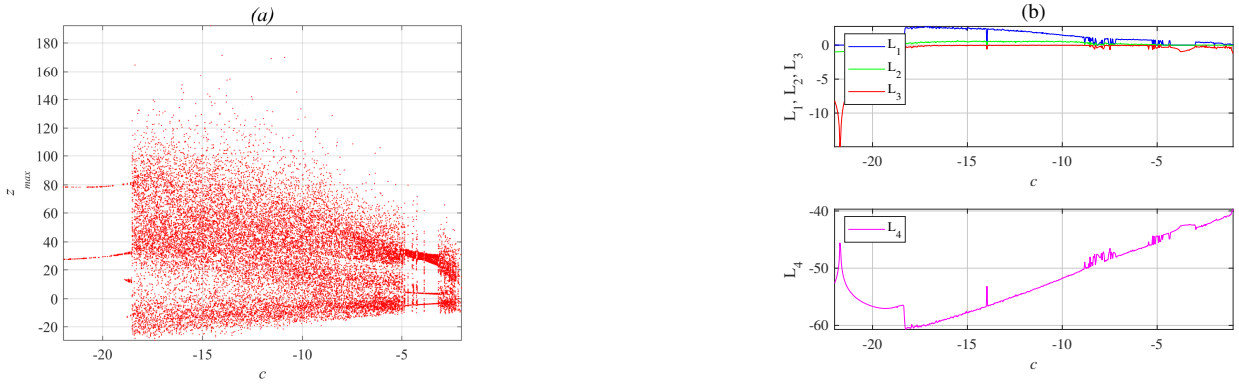

FIG. 1. Dynamical analysis of system (2) with $a = 50$, $b = 10$, $d = 0.2$, $e = 10$, $f = 16$, and $g = 0.5$: (a) Bifurcation diagram with respect to c; (b) Lyapunov exponents spectrum with respect to c.

that the system (2) exhibits hyperchaotic behavior, excepting the appearance of certain periodic windows near $c = -7.88$, $c = -5.14$, $c = -4.51$, and $c = -3.59$. In these zones, we have $L_1 = 0$, $L_2 = 0$, $L_3 < 0$, and $L_4 < 0$, which indicates that system (2) exhibits regular dynamics, and the chaotic motions have been lost. Finally, as $c \in (-3.59, -1]$, system (2) exhibits chaotic behavior, in which $L_1 > 0$, $L_2 = 0$, $L_3 < 0$, and $L_4 < 0$. According to the bifurcation diagram shown in Fig. 1(a), it is obvious that, starting with the periodic area, an increase leads the state z to undergo a transition into hyperchaos and then into certain periodic areas and finally to chaos. To further investigate the dynamics of the novel 4D system, several phase portraits of system (2) with $c = -16$ in 2D and 3D projections are shown in Fig. 2. A four-wing hyperchaotic attractor is observed for this set of parameters. Additionally, for $c = -3.59$, phase portraits of system (2) are shown in Fig. 3. In this case, a periodic circle is observed, indicating regular dynamics. Thus, system (2) has rich dynamic behaviors.

To further estimate the complexity of the new 4D system, the Kaplan-Yorke dimension, which is based on the dynamics of the Lyapunov exponents, is computed in this study.

Definition 1. *The Kaplan-Yorke dimension is defined as [26]*

$$D_{KY} = j + \frac{\sum_{i=1}^{j} L_i}{|L_{j+1}|}, \tag{13}$$

where j is the largest integer in which $\sum_{i=1}^{j} L_i > 0$ and $\sum_{i=1}^{j+1} L_i < 0$.

The calculations of Lyapunov exponents and Kaplan-Yorke dimensions were conducted at $0.1s$ intervals for an overall time of $1000s$. The results of numerical simulations are shown in Table 2.

TABLE 2. Parameter estimation results

c	L_1	L_2	L_3	L_4	D_{KY}	Dynamical state
-22	0	-0.976	-8.746	-51.996	1	Periodic
-18.27	2.534	0.277	-0.329	-60.538	3.041	Hyperchaotic
-16	2.567	0.543	-0.055	-58.867	3.052	Hyperchaotic
-3.59	0	0	-0.892	-42.505	1	Periodic
-1	0.241	0	-0.741	-40.176	2.325	Chaotic

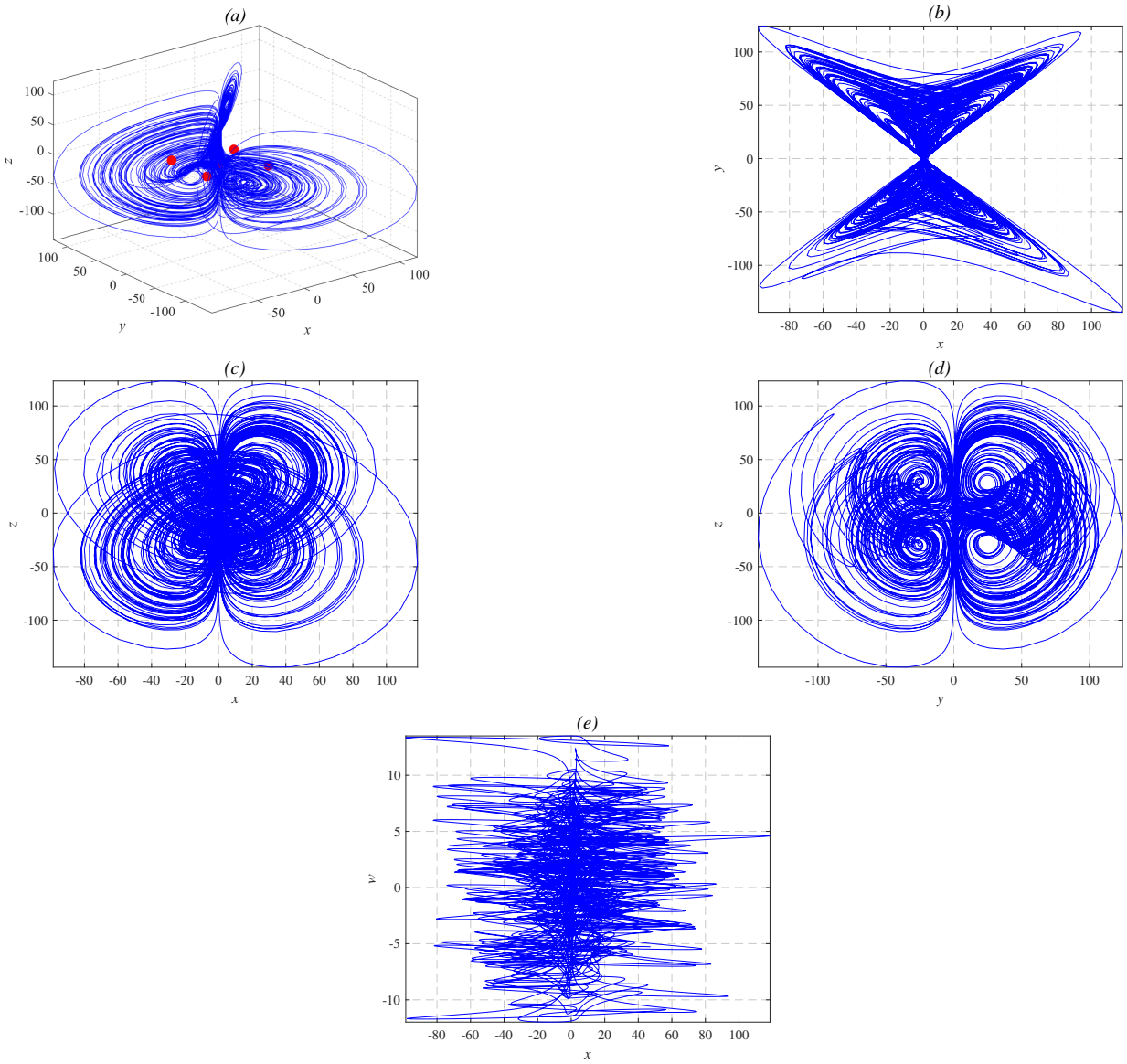

FIG. 2. Phase portrait of system (2) with $a = 50$, $b = 10$, $c = -16$, $d = 0.2$, $e = 10$, $f = 16$, and $g = 0.5$: (a) in (x, y, z)-space; (b) in (x, y)-plane; (c) in (x, z)-plane; (d) in (y, z)-plane; (e) in (x, w)-plane.

The Poincaré section technique, known for its practicality, provides a further tool for differentiating a chaotic behavior from a regular one. A Poincaré section can be utilized to transform a higher-dimensional continuous system into a discrete map of reduced dimension. To construct the Poincaré section, we use a suitable Poincaré section Ω given by

$$\begin{aligned}
\Sigma_1 &= \left\{[x, y, z, w]^T \in \mathbb{R}^4 \mid x = -5\right\} \\
\Sigma_2 &= \left\{[x, y, z, w]^T \in \mathbb{R}^4 \mid y = 0\right\} \\
\Sigma_3 &= \left\{[x, y, z, w]^T \in \mathbb{R}^4 \mid z = 0\right\} \\
\Sigma_4 &= \left\{[x, y, z, w]^T \in \mathbb{R}^4 \mid w = 0\right\}
\end{aligned} \tag{14}$$

Poincaré sections of the new system (2) are depicted in Fig. 4 for better analysis of the hyperchaotic behavior.

2.5. Multistability and coexisting attractors

Multistability is a complicated phenomenon frequently observed in chaotic systems, which features the coexistence of multiple periodic, chaotic, and hyperchaotic attractors under the same system parameters but different initial conditions. This study demonstrates that the new 4D system (2) displays multistability with coexisting attractors for different initial conditions.

Case 1. Coexistence of two periodic attractors.

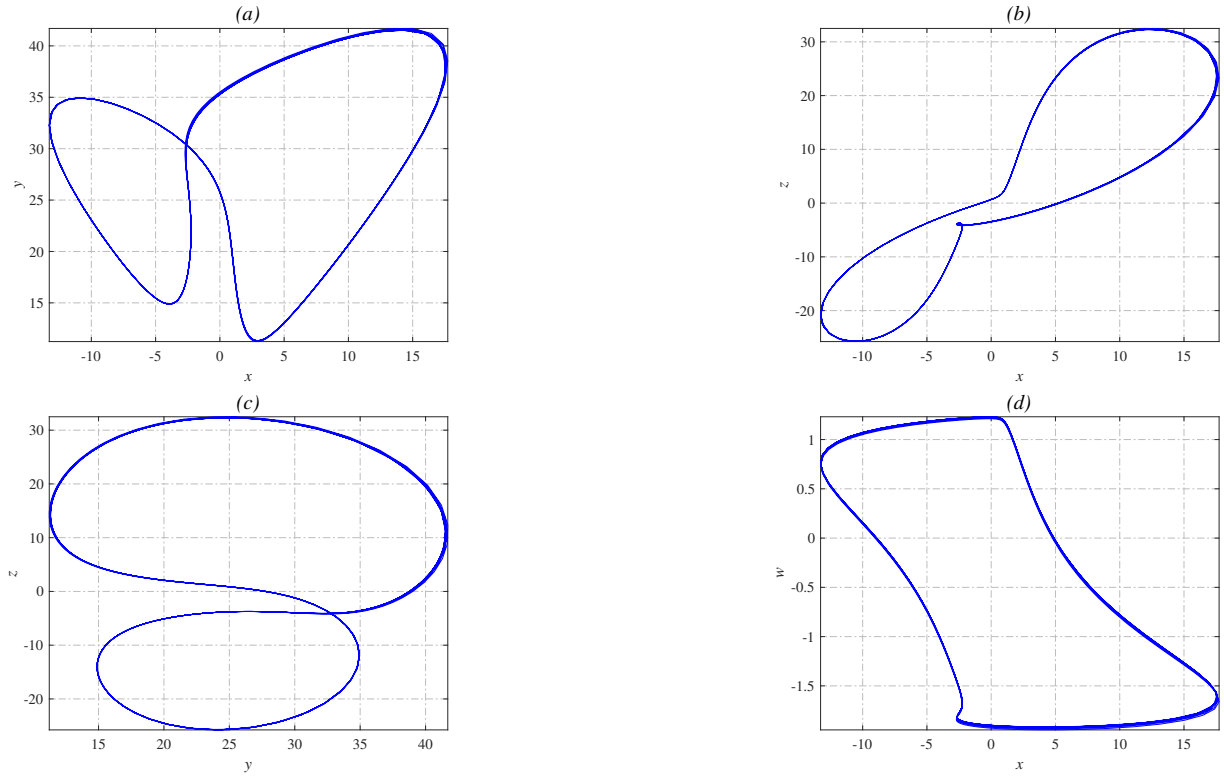

FIG. 3. Phase portrait of system (2) with $a = 50$, $b = 10$, $c = -3.59$, $d = 0.2$, $e = 10$, $f = 16$, and $g = 0.5$: (a) in (x, y)-plane; (b) in (x, z)-plane; (c) in (y, z)-plane; (d) in (x, w)-plane.

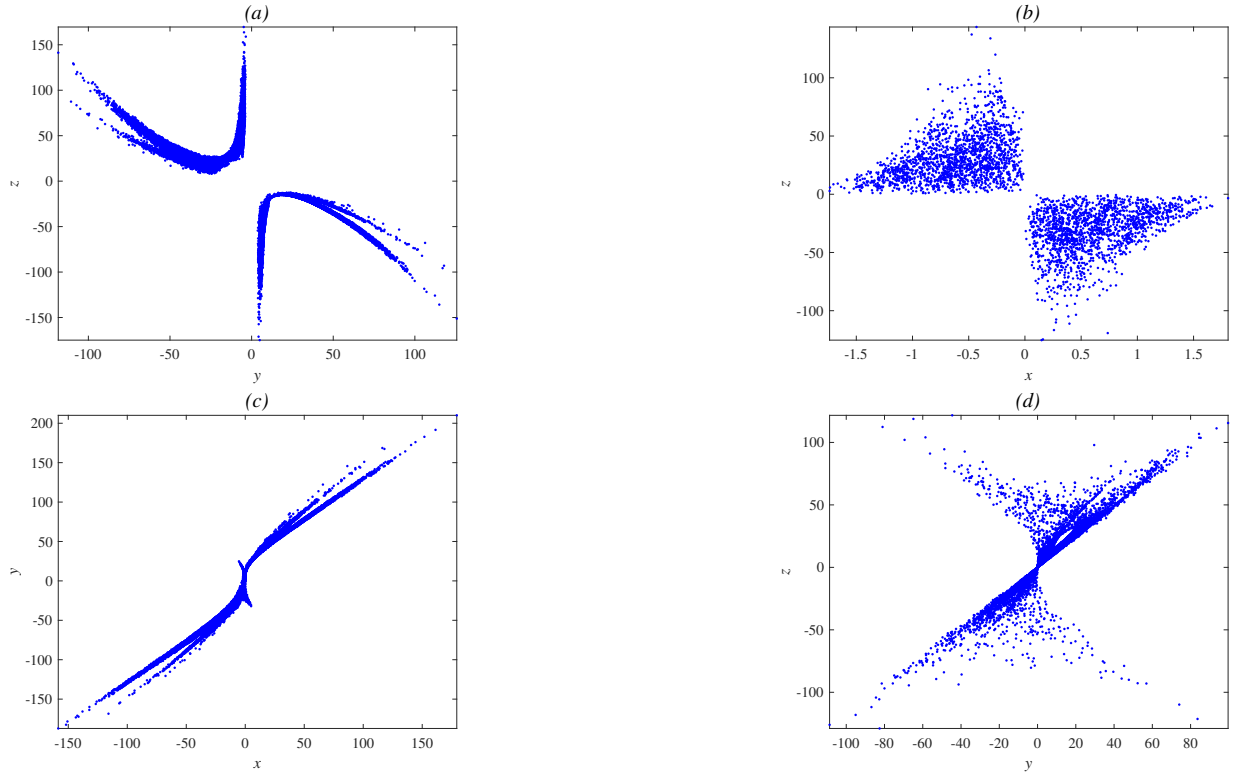

FIG. 4. Poincaré sections of system (2): (a) projection on (y, z)-plane when Poincaré section is $x = -5$; (b) projection on (x, z)-plane when Poincaré section is $y = 0$; (c) projection on (x, y)-plane when Poincaré section is $z = 0$; (d) projection on (y, z)-plane when Poincaré section is $w = 0$.

Fix the parameters as $a = 50$, $b = 10$, $c = -22$, $d = 0.2$, $e = 10$, $f = 16$, and $g = 0.5$. The 4D system (2) exhibits a coexistence of two periodic attractors. For initial conditions $(x_0, y_0, z_0, w_0) = (1, 1, 1, 1)$, the Lyapunov exponents are estimated as $L_1 = 0$, $L_2 = -0.976$, $L_3 = -8.746$, and $L_4 = -51.996$, with the Kaplan-Yorke fractal dimension $D_{KY} = 1$. The corresponding periodic attractor is plotted in Fig. 5(a). For initial conditions $(x_0, y_0, z_0, w_0) = (-1, 1, 1, -1)$, the

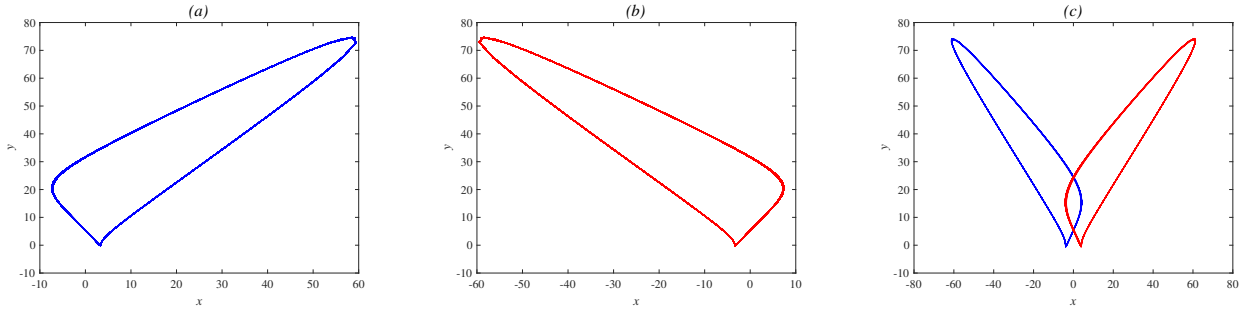

FIG. 5. Two coexisting periodic attractors of system (2) with parameters $a = 50$, $b = 10$, $c = -22$, $d = 0.2$, $e = 10$, $f = 16$, and $g = 0.5$.

Lyapunov exponents are estimated as $L_1 = 0$, $L_2 = -0.976$, $L_3 = -7.968$, and $L_4 = -51.996$, with the Kaplan-Yorke fractal dimension $D_{KY} = 1$. The corresponding periodic attractor is plotted in Fig. 5(b). In Fig. 5(c), the 4D system (2) illustrates the coexistence of two periodic attractors.

Case 2. Coexistence of two hyperchaotic attractors.

Fix the parameters as $a = 50$, $b = 10$, $c = -14$, $d = 0.2$, $e = 10$, $f = 16$, and $g = 0.5$. The novel 4D system (2) exhibits a coexistence of two four-wing hyperchaotic attractors that are symmetrical with respect to y-axis. For initial conditions $(x_0, y_0, z_0, w_0) = (1, 1, 1, 1)$, the Lyapunov exponents are estimated as $L_1 = 2.417$, $L_2 = 0.573$, $L_3 = -0.021$, and $L_4 = -55.163$, with the Kaplan-Yorke fractal dimension $D_{KY} = 3.054$. The corresponding four-wing hyperchaotic attractor is plotted in Fig. 6(a). For initial conditions $(x_0, y_0, z_0, w_0) = (-1, 1, 1, -1)$, the Lyapunov

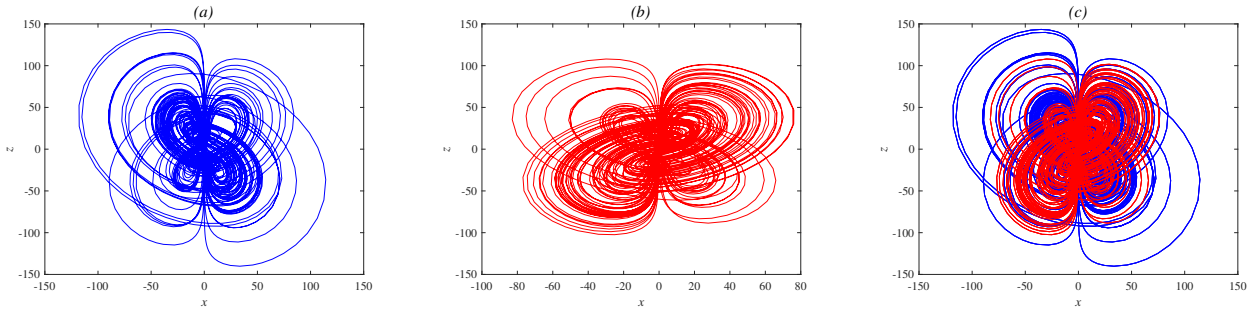

FIG. 6. Two coexisting four-wing hyperchaotic attractors of system (2) with parameters $a = 50$, $b = 10$, $c = -14$, $d = 0.2$, $e = 10$, $f = 16$, and $g = 0.5$.

exponents are estimated as $L_1 = 2.398$, $L_2 = 0.539$, $L_3 = -0.013$, and $L_4 = -55.073$, with the Kaplan-Yorke fractal dimension $D_{KY} = 3.053$. The corresponding four-wing hyperchaotic attractor is plotted in Fig. 6(b). In Fig. 6(c), the 4D system (2) illustrates the coexistence of two four-wing hyperchaotic attractors.

Case 3. Coexistence of two chaotic attractors.

Fix the parameters as $a = 50$, $b = 10$, $c = -6$, $d = 0.2$, $e = 10$, $f = 16$, and $g = 0.5$. The novel 4D system (2) exhibits a coexistence of two double-wing chaotic attractors that are symmetrical with respect to y-axis. For initial conditions $(x_0, y_0, z_0, w_0) = (1, 1, 1, 1)$, the Lyapunov exponents are estimated as $L_1 = 0.774$, $L_2 = 0$, $L_3 = -0.063$, and $L_4 = -45.884$, with the Kaplan-Yorke fractal dimension $D_{KY} = 3.015$. The corresponding double-wing chaotic attractor is plotted in Fig. 7(a). For initial conditions $(x_0, y_0, z_0, w_0) = (-1, 1, 1, -1)$, the Lyapunov exponents are estimated as $L_1 = 0.845$, $L_2 = 0$, $L_3 = -0.071$, and $L_4 = -45.918$, with the Kaplan-Yorke fractal dimension $D_{KY} = 3.017$. The corresponding double-wing chaotic attractor is plotted in Fig. 7(b). In Fig. 7(c), the 4D system (2) illustrates the coexistence of two double-wing chaotic attractors.

3. Implementation of chaos-based audio cryptosystem

Chaos encryption is a common field of study due to its nonlinearity, real-time efficiency, security, resistance to disturbance, and shortness of key length. Hyperchaotic encryption provides enhanced security due to its rich dynamical properties and higher randomness. It exhibits a broad spectrum and frequency of disturbances, which makes it robust

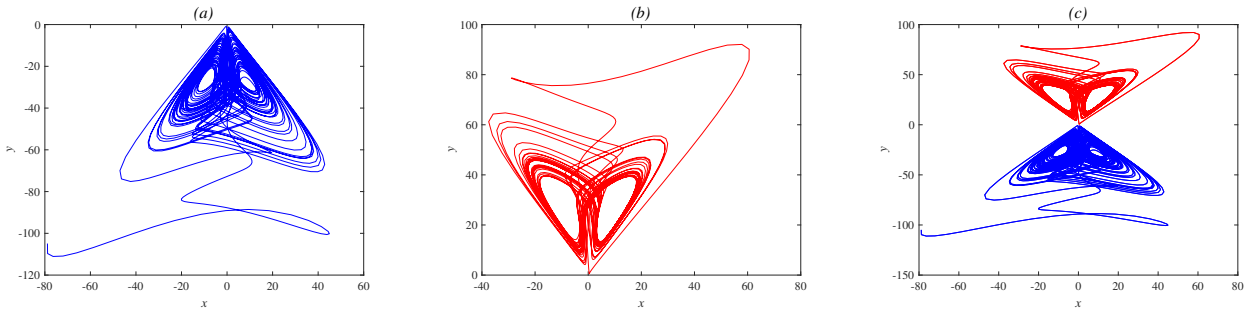

FIG. 7. Two coexisting double-wing chaotic attractors of system (2) with parameters $a = 50$, $b = 10$, $c = -6$, $d = 0.2$, $e = 10$, $f = 16$, and $g = 0.5$.

against noise attacks. Hyperchaotic systems display rich dynamical behaviors and show high complexity, thereby rendering the encryption technique more straightforward and realistic. Customer data leaking has become known as a serious security issue due to weaknesses in the network's transmission processes. Consequently, addressing this issue requires the use of information encryption technological advances.

In this section, a secure audio encryption algorithm that uses a hyperchaotic key sequence is proposed, in which the new hyperchaotic system (2) is used in the simulations. This algorithm uses the 4D hyperchaotic system and XOR operation $\oplus$ to secure audio signals with two layers of encryption, and then it has a synchronized decryption process to get back the original audio. Below is a detailed review.

3.1. Encryption process

The encryption has two consecutive phases: chaotic scrambling and dynamic masking, both using state variables generated by the hyperchaotic system. Figure 8 shows the framework of the proposed audio cryptosystem. The original audio signal is initially masked by employing a key stream produced through the XOR operation of a random sequence derived from the novel 4D hyperchaotic system, as outlined in Algorithm 1 (see Appendix A.1). Subsequently, the masked signal is further encrypted utilising key streams generated as depicted in Fig. 8(a), applying Algorithm 2 (see Appendix A.2). The scrambled audio signal is then sent via a public channel to the receiver.

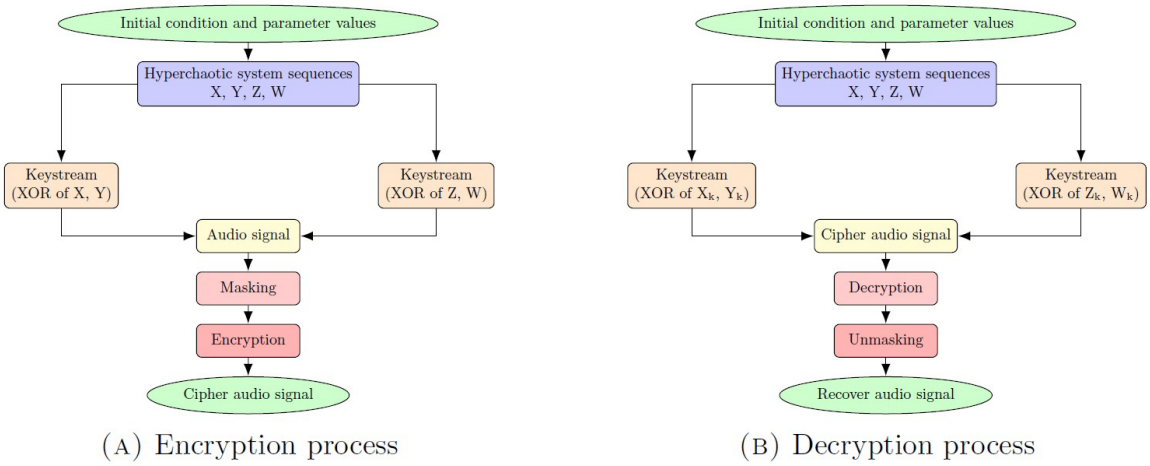

FIG. 8. Flowchart of the proposed audio cryptosystem: (a) Encryption process; (b) Decryption process.

3.2. Decryption process

The decryption process follows the same flowchart and procedures as the encryption process for recovering the original audio signal as stated in Algorithm 3 (see Appendix A.3). The proposed cryptographic approach is symmetric, using the same key for both the encryption and decryption of the audio signal. Figure 8(b) illustrates the audio decryption flowchart process.

4. Experiments and security analysis

Simulation results were conducted using MATLAB software to analyze the performance and security resistance of the system that was constructed. Tests included waveform analyses, percentage residual deviation (PRD), signal-to-noise ratio

(SNR), and correlation coefficient measurements [27]. Audio inputs were recorded at $8,000$ Hz with an 8-bit quantization level. Figures 9(a), 9(c), and 9(e) show the waveforms of the original, encrypted, and decrypted audio signals, respectively. Additionally, their corresponding histogram distributions are shown in Figs. 9(b), 9(d), and 9(f), respectively. The

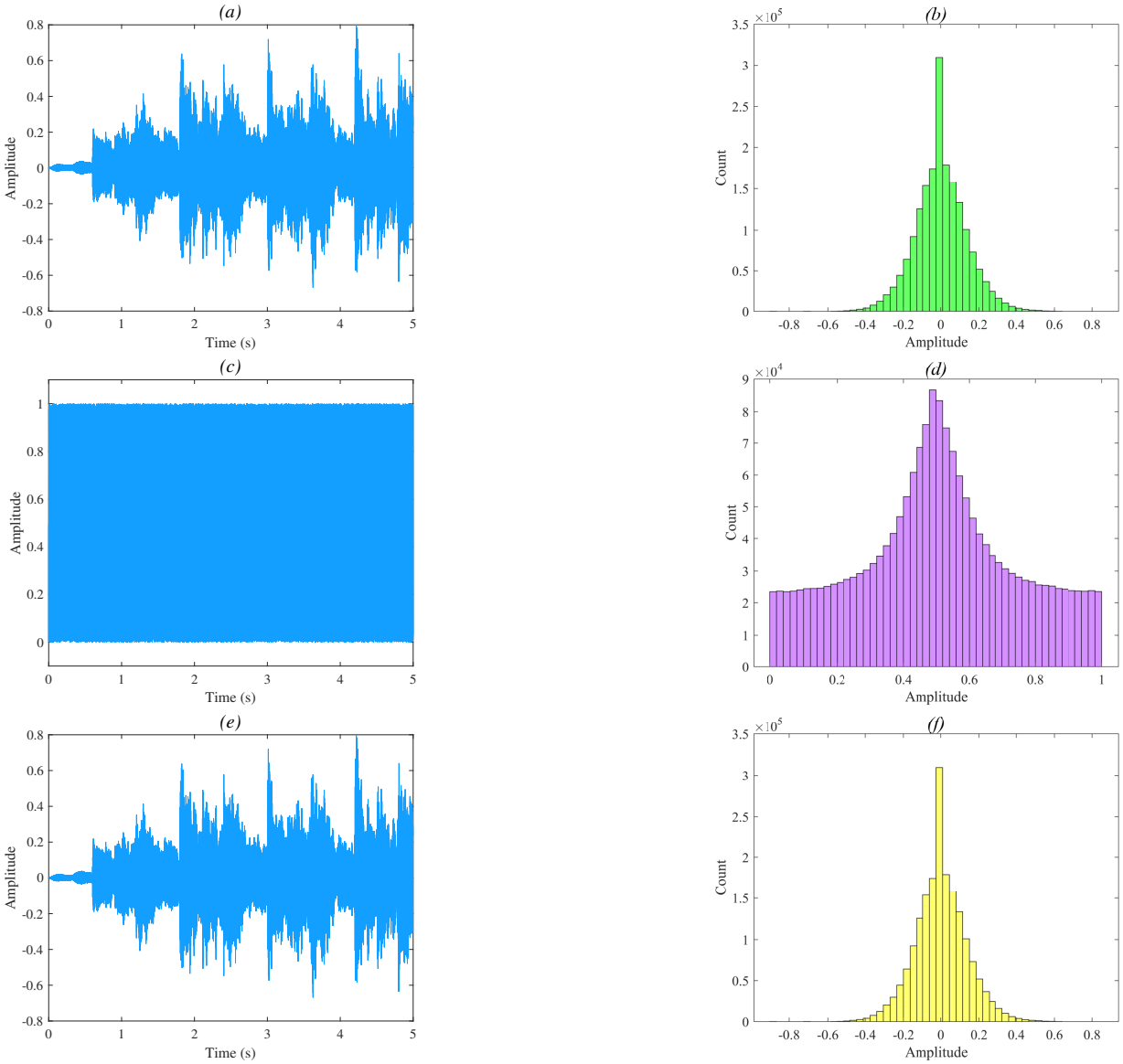

FIG. 9. Simulation results of audio encryption: (a) Original audio signal; (b) Histogram of (a); (c) Encrypted audio signal; (d) Histogram of (c); (e) Decrypted audio signal; (f) Histogram of (e).

encrypted waveform exhibits less resemblance to the original, but the decrypted output accurately captures the structure of the original signal. The findings indicate that the proposed method efficiently withstands statistical cryptanalysis, providing reliable security for audio communication networks. The technique transforms structured data into noise-like outputs, displaying functional reliability and enhanced security for needed audio transmissions. In the histogram distributions of three signals, the encrypted data exhibits consistent unpredictability in stark contrast to the Gaussian-like patterns of the original and decrypted signals, potentially introducing weaknesses. This statistical disparity underscores the encryption scheme's capacity to counter frequency-based attacks.

Frequency domain analysis is also necessary to verify the accuracy of the encryption, despite the obvious disparity of the original and encrypted audios in the time domain. For better quantitative analysis, Figs. 10(a), 10(b), and 10(c) illustrate the frequency spectra of the original, encrypted, and decrypted audio signals, respectively. As can be observed, the frequency spectra of the decrypted and original audio signals are indistinguishable. The spectrum of the encrypted audio data has a homogenous distribution and is entirely distinct from both the original and decrypted audio. The encryption and decryption processes are carried out without loss of information, and the encryption process is considered successful. The study demonstrates that the new proposed hyperchaotic system is suitable for encryption applications.

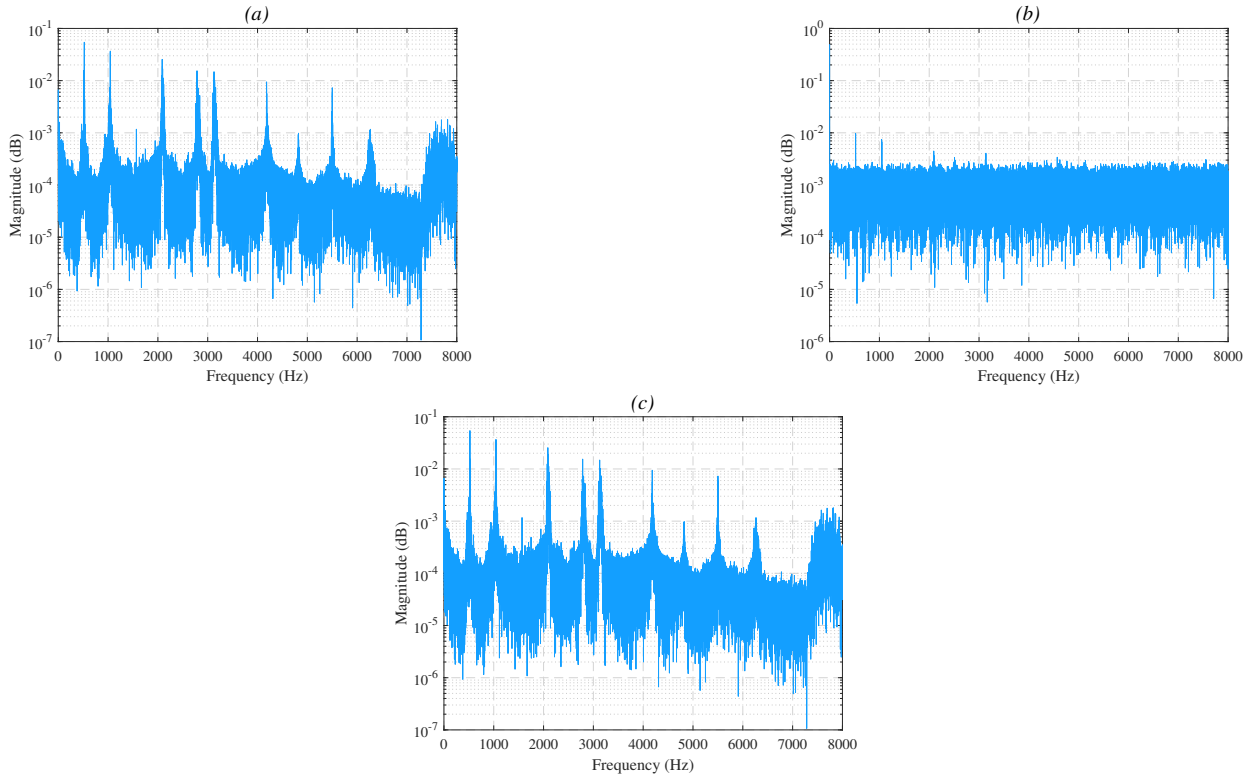

FIG. 10. Frequency spectra of audio signals: (a) Original audio spectrum, (b) Encrypted audio spectrum, (c) Decrypted audio spectrum

A statistical analysis of both the encryption and decryption procedures was carried out using four different techniques: percentage residual deviation (PRD), signal noise ratio (SNR), entropy, and correlation. The findings are shown in Table 3. These findings indicate that the encryption and decryption processes are fairly efficient. The PRD is an estimation tool utilized to quantify the divergence between encrypted and original audio signals. Low PRD values imply good accuracy and low dispersion, while high PRD values imply large disparities. The signal noise ratio (SNR) is a quantitative metric that measures the intensity of the original audio stream. The correlation coefficient indicates the level of quality of the encrypted audio signals. High PRD values suggest large deviation, and large negative SNR values suggest more noise power relative to signal power. Near-zero correlation values suggest less resemblance between encrypted and original signals.

TABLE 3. The measurements of statistical metrics between the original and encrypted audio signals

File name	Size	Duration (Sec.)	PRD	SNR (dB)	Entropy	Correlation
Audio-1	896 KB	3.98	1.4285×10^5	-64.3176	7.9754	0.0013

5. Conclusion

The study presented a novel four-wing hyperchaotic system developed from the 3D chaotic Qi system. The system's behavior is studied using various numerical tools, including phase plots, bifurcation diagrams, Lyapunov exponent spectra, and Poincaré sections. It is shown that this system can exhibit complex behavior, including periodic, chaotic, and hyperchaotic patterns across various parameters. It also displays known dynamical characteristics, such as multistability and coexistence of attractors under identical parameter values but different initial conditions. An efficient audio encryption algorithm has been developed, demonstrating its performance, accuracy, and security against various attacks.

Future studies can include the 4D hyperchaotic system with quantum-resistant cryptography for the enhancement of secure nanosensors. Utilizing it in neuromorphic nanochips could offer energy-efficient, real-time audio encryption inside edge computing. The combination of chaotic dynamics with nanophotonics can improve ultrafast encryption for healthcare or military data. Employing chaotic and hyperchaotic vibrations of nanobeams in signal transmission can also enhance security [28]. Meanwhile, the complex dynamical behavior of the lipidic nanoparticles, such as liposomes, can be used in developing various secure communication schemes, providing high accuracy and satisfactory performance [29]. Optimization of machine learning may further improve adaptive security in dynamic nanoelectronics.

Appendix

A.1

Algorithm 1 Key generation using the novel hyperchaotic system (2)

1: Generate hyperchaotic sequences $X = [x_1, x_2, \ldots, x_n]$, $Y = [y_1, y_2, \ldots, y_n]$, $Z = [z_1, z_2, \ldots, z_n]$, and $W = [w_1, w_2, \ldots, w_n]$ by solving Eq. (2) of system
2: Quantize sequences:

$$X_k = \text{mod}(\text{round}(X \times 10^{20}), 2^{16}),$$
$$Y_k = \text{mod}(\text{round}(Y \times 10^{20}), 2^{16}),$$
$$Z_k = \text{mod}(\text{round}(Z \times 10^{20}), 2^{16}),$$
$$W_k = \text{mod}(\text{round}(W \times 10^{20}), 2^{16})$$

3: Convert X_k, Y_k, Z_k, W_k to binary
4: Generate keys via XOR:

$$\text{Key1} = X_k \oplus Y_k,$$
$$\text{Key2} = Z_k \oplus W_k$$

5: **repeat**
6: Iterate and append new key bits
7: **until** Key length matches plaintext

A.2

Algorithm 2 Audio encryption using the 4D hyperchaotic system (2)

1: Read audio file A, convert to binary
2: First encryption: $En1 = A \oplus$ Key1
3: Second encryption: $En = En1 \oplus$ Key2
4: **repeat**
5: Process subsequent segments
6: **until** Entire file is encrypted
7: Output cipher audio file

A.3

Algorithm 3 Audio decryption using the 4D hyperchaotic system (2)

1: Read cipher audio file En
2: First decryption: $En1 = En \oplus$ Key2
3: Second decryption: $A = En1 \oplus$ Key1
4: Reconstruct original audio signal

References

[1] Poincaré H. Sur le problème des trois corps et les équations de la dynamique. *Acta mathematica*, 1890, **13**(1), P. A3–A270.
[2] Lorenz E.N. Deterministic nonperiodic flow. *Journal of the Atmospheric Sciences*, 1963, **20**(2), P. 130–141.
[3] Zambrano-Serrano E., Anzo-Hernández A. A novel antimonotic hyperjerk system: Analysis, synchronization and circuit design. *Physica D: Nonlinear Phenomena*, 2021, **424**, P. 132927.
[4] Zhang S., Zheng J., Wang X., Zeng Z. A novel no-equilibrium HR neuron model with hidden homogeneous extreme multistability. *Chaos, Solitons & Fractals*, 2021, **145**, P. 110761.
[5] Yan M., Xu H. The multi-scroll hyper-chaotic coexistence attractors and its application. *Signal Processing: Image Communication*, 2021, **95**, P. 116210.
[6] Bao B., Peol M.A., Bao H., Chen M., Li H., Chen B. No-argument memristive hyper-jerk system and its coexisting chaotic bubbles boosted by initial conditions. *Chaos, Solitons & Fractals*, 2021, **144**, P. 110744.
[7] Haneche N., Hamaizia T. A three-dimensional discrete fractional-order HIV-1 model related to cancer cells, dynamical analysis and chaos control. *Mathematical Modelling and Numerical Simulation with Applications*, 2024, **4**(3), P. 256–279.
[8] Haneche N., Hamaizia T. Modified generalized projective synchronization of the geomagnetic Krause and Robert fractional-order chaotic system and its application in secure communication. *The European Physical Journal B*, 2025, **98**(4), P. 56.
[9] Haneche N., Hamaizia T. Nonlinear Dynamics of Fractional-Order Chaotic Chemical Reactor System Based on the Adomian Decomposition Method and Its Control via Adaptive Sliding Mode Control. *MATCH Communications in Mathematical and in Computer Chemistry*, 2025, **94**(2), P. 355–384.

[10] Fedorov E.G. Properties of an oriented ring of neurons with the FitzHugh-Nagumo model. *Nanosystems: Physics, Chemistry, Mathematics*, 2021, **12**(5), P. 553–562.
[11] Mikhaylov A.S., Mikhaylov V.S. On the construction of de Branges spaces for dynamical systems associated with finite Jacobi matrices. *Nanosystems: Physics, Chemistry, Mathematics*, 2022, **13**(1), P. 24–29.
[12] Matrasulova J., Yusupovb J.R., Saidov A.A. Fast forward evolution in heat equation: Tunable heat transport in adiabatic regime. *Nanosystems: Physics, Chemistry, Mathematics*, 2023, **14**(4), P. 421–427.
[13] Ni X., Ying L., Lai Y.C., Do Y. Complex dynamics in nanosystems. *Physical Review E–Statistical, Nonlinear, and Soft Matter Physics*, 2013, **87**(5), P. 052911.
[14] Lambruschini C.L., Jaimes-Reátegui R., Huerta-Cuéllar G. Dynamics near the edge-of-chaos in a fiber laser model. *Physics Letters A*, 2023, **481**, P. 128995.
[15] Zhang X., Li C., Iu H.H., Zhao L., Yang Y. A chaotic memristive Hindmarsh-Rose neuron with hybrid offset boosting. *Chaos, Solitons & Fractals*, 2024, **185**, P. 115150.
[16] Zhang G., Li C., Xiong X. Analysis and comparison of four signal processing schemes for noise reduction in chaotic communication systems and application of LDPC code. *Chaos, Solitons & Fractals*, 2024, **186**, P. 115184.
[17] Haneche N., Hamaizia T. A secure communication scheme based on generalized modified projective synchronization of a new 4-D fractional-order hyperchaotic system. *Physica Scripta*, 2024, **99**(9), P. 095203.
[18] Teng L., Wang X., Yang F., Xian Y. Color image encryption based on cross 2D hyperchaotic map using combined cycle shift scrambling and selecting diffusion. *Nonlinear Dynamics*, 2021, **105**(2), P. 1859–1876.
[19] Jahanshahi H., Yousefpour A., Munoz-Pacheco J.M., Kacar S., Pham V.T., Alsaadi F.E. A new fractional-order hyperchaotic memristor oscillator: Dynamic analysis, robust adaptive synchronization, and its application to voice encryption. *Applied Mathematics and Computation*, 2020, **383**, P. 125310.
[20] Fu S., Cheng X., Liu J. Dynamics, circuit design, feedback control of a new hyperchaotic system and its application in audio encryption. *Scientific Reports*, 2023, **13**(1), P. 19385.
[21] Benkouider K., Sambas A., Bonny T., Al Nassan W., Moghrabi I.A., Sulaiman I.M., Hassan B.A., Mamat M. A comprehensive study of the novel 4D hyperchaotic system with self-exited multistability and application in the voice encryption. *Scientific Reports*, 2024, **14**(1), P. 12993.
[22] Xiong L., Yang F., An X., Zhang X. Hyperchaotic system with application to image encryption. *International Journal of Bifurcation and Chaos*, 2022, **32**(13), P. 2250191.
[23] Zhou S., Yin Y., Erkan U., Toktas A., Zhang Y. Novel hyperchaotic system: Implementation to audio encryption. *Chaos, Solitons & Fractals*, 2025, **193**, P. 116088.
[24] Qi G., Chen G., Van Wyk M.A., Van Wyk B.J., Zhang Y. A four-wing chaotic attractor generated from a new 3-D quadratic autonomous system. *Chaos, Solitons & Fractals*, 2008, **38**(3), P. 705–721.
[25] Wolf A., Swift J.B., Swinney H.L., Vastano J.A. Determining Lyapunov exponents from a time series. *Physica D: Nonlinear Phenomena*, 1985, **16**(3), P. 285–317.
[26] Kaplan J.L., Yorke J.A. Chaotic Behavior of Multidimensional Difference Equations, *Lecture Notes in Mathematics*, Springer, Berlin Heidelberg, 1979, P. 204–227.
[27] Haridas T., Upasana S.D., Vyshnavi G., Krishnan M.S., Muni S.S. Chaos-based audio encryption: Efficacy of 2D and 3D hyperchaotic systems. *Franklin Open*, 2024, **8**, P. 100158.
[28] Yakovleva T.V., Awrejcewicz J., Kruzhilin V.S., Krysko V.A. On the chaotic and hyper-chaotic dynamics of nanobeams with low shear stiffness. *Chaos: An Interdisciplinary Journal of Nonlinear Science*, 2021, **31**(2), P. 023107.
[29] Naziris N., Chountoulesi M., Stavrinides S., Hanias M., Demetzos C. Chaotic dynamics and stability of liposomal nanosystems. *Current Nanoscience*, 2022, **18**(3), P. 375–390.

Submitted 12 April 2025; revised 29 May 2025; accepted 30 May 2025

Information about the authors:

Nabil Haneche – Applied Mathematics and Modeling Laboratory, Department of Mathematics, University of Mentouri Brothers, Constantine, 25000, Algeria; ORCID 0009-0005-2866-6853; nabil.haneche@doc.umc.edu.dz

Tayeb Hamaizia – Mathematical Modeling and Simulation Laboratory, Department of Mathematics, University of Mentouri Brothers, Constantine, 25000, Algeria; ORCID 0000-0001-8507-572X; el.tayyeb@umc.edu.dz

Conflict of interest: the authors declare no conflict of interest.